11th Australasian Fluid Mechanics Conference
University of Tasmania, Hobart, Australia
14-18 December 1992

TURBULENCE SPECTRA IN THE NEAR-WALL REGION

S.M. HENBEST[1], J.D. LI[2] and A.E. PERRY[2]

[1]Aeronautical Research Laboratory, DSTO, 506 Lorimer St, Fishermens Bend, VIC 3207, AUSTRALIA

[2]Dept Mechanical & Manufacturing Engineering, University of Melbourne, Parkville, VIC 3052, AUSTRALIA

1. ABSTRACT

In this paper, the dimensional analysis approach of Perry, Henbest & Chong (1986) [*PHC*] has been extended to turbulence spectra in the near-wall-region of a zero pressure gradient smooth-wall turbulent boundary layer and of fully developed smooth-wall pipe flow. Near-wall-region pipe flow and boundary layer spectral data are presented.

2. INTRODUCTION

The kinematic aspects of coherent structures in the near-wall-region have been studied extensively (Robinson, 1991). Smith *et al.* (1991) have reviewed the dynamic characteristics of these structures. The majority of turbulence production in boundary layers occurs in the buffer region during intermittent, violent outward ejections of low-speed fluid and during inward sweeping of high-speed fluid. The low-speed fluid ejections carry with them small scale, wall-affected viscous motions. The fine scale details of the low-speed ejections initially depend on the viscous length scale; as the low speed fluid moves away from the wall a competing process exists between viscous diffusion and local mean stretching of the vortex ejections; eventually, in the fully-turbulent-region the initial viscous length scale is forgotten and small scale motions depend on the local energy dissipation and the fluid viscosity and so scale with Kolmogorov (1941) scaling. These Kolmogorov motions are convected towards the wall by the large scale "sweeping" motions.

The coordinate system used here is x for the streamwise direction, y for the spanwise direction and z for the distance normal from the wall. U_∞ is the free stream velocity, while, u_1, u_2 and u_3 are the streamwise, spanwise and normal fluctuating velocity components, respectively. In this paper, the near-wall-region is defined to be $z^+ = zU_\tau/\nu \leq 150$, and the turbulent-wall-region to be $z^+ \geq 150$ and $z/\Delta \leq 0.15$, where U_τ is the wall shear velocity, ν is the kinematic viscosity and Δ is the boundary layer thickness or pipe radius.

3. DIMENSIONAL ANALYSIS OF NEAR-WALL TURBULENCE SPECTRA

Perry & Abell (1975,1977) [*PA*] used dimensional analysis to study wall turbulence in pipes. One of the lessons to be learnt from *PA* was that dimensional analysis cannot be applied to broadband turbulent intensities; rather, it should be applied to the wavenumber domain of turbulence spectra. Perry & Chong (1982) [*PC*] used physical reasoning, based on the Townsend (1976) attached eddy hypothesis, to develop a model for wall turbulence together with a consistent dimensional analysis argument for the spectra of velocity fluctuations in fully turbulent flow. This work was extended in *PHC* and the pipe flow spectral data presented gave excellent support for the attached eddy hypothesis. *PA, PC, PHC* considered flow in the fully-turbulent-region with particular emphasis on the turbulent-wall-region and did not include the near-wall-region. Henbest (1983) considered near-wall streamwise spectra in fully developed turbulent pipe flow.

Let $\phi_{ij}(k_1)$ denote the cross-power spectral densities per unit streamwise wavenumber k_1 for the velocity fluctuations u_i and u_j. $\phi_{ij}(k_1)$ are normalised as follows

$$\int \phi_{ij}(k_1)\, dk_1 = \overline{u_i u_j}\,, \qquad (1)$$

where i and j may equal 1, 2 or 3 and repeated indices do not denote a summation.

In the near-wall-region of pipe or boundary layer flow the following analysis should apply. At high wavenumbers, small scale viscous motions should dominate over Kolmogorov motions and ϕ_{11}, ϕ_{22} ϕ_{33} and ϕ_{13} should follow viscous scaling, *ie.*,

$$\frac{\phi_{ij}(k_1\nu/U_\tau)}{U_\tau^2} = h_{ij}(k_1\nu/U_\tau) = \frac{\phi_{ij}(k_1)}{\nu U_\tau}. \qquad (2)$$

Eddies of scale $\delta = O(z)$ will contribute energy at moderate wavenumbers - these motions are sometimes called "active motions" - and ϕ_{11}, ϕ_{22}, ϕ_{33} and ϕ_{13} should follow inner-flow scaling,

$$\frac{\phi_{ij}(k_1 z)}{U_\tau^2} = g_{ij}(k_1 z) = \frac{\phi_{ij}(k_1)}{zU_\tau^2}\,. \qquad (3)$$

Eddies of scale $\delta \gg z$ through to eddies of scale $\delta = O(\Delta)$ will contribute energy at low wavenumbers **only** to u_1- and u_2-motions; these motions are sometimes referred to as "inactive motions". ϕ_{11}, ϕ_{22} should follow outer-flow scaling and depend on the large scale flow geometry, *ie.*,

$$\frac{\phi_{ij}(k_1\Delta)}{U_\tau^2} = f_{ij}(k_1\Delta) = \frac{\phi_{ij}(k_1)}{\Delta U_\tau^2}. \qquad (4)$$

In §4 near-wall pipe flow spectra of Henbest (1983) are presented. In §5 the current boundary layer experiment is detailed and spectral results are presented in §6.

4. NEAR-WALL PIPE FLOW SPECTRA

The smooth-wall pipe flow ϕ_{11}-spectra of Henbest (1983) are shown in Figure 1. These spectra were measured in the near-wall-region over a range of z^+ from 20.8 to 136 and a range of z/Δ from 0.01 to 0.06 (see *PHC* for details of the experimental set-up). The Reynolds number (based on pipe diameter and centerline velocity) varied from 75,000 to 200,000. In Figure 1a the spectra are presented with outer-

flow scaling (4); the collapse of the data at low $k_1\Delta$ is fair and improves in the region where the spectra collapse to an inverse power law distribution (see *PHC*). In Figure 1b the same spectra are presented with inner-flow scaling (3), the data collapse at moderate $k_1 z$ and an inverse power law region is also apparent. Given the collapse of the data in Figure 1a to an inverse power law region, the collapse of the data in Figure 1b to an inverse power law distribution is expected since the change in scaling from outer-flow to inner-flow is achieved by translating each spectrum along a line of slope equal to -1 when using log-log axes. The same data are plotted with viscous scaling (2) in Figure 1c. The collapse at high wavenumbers is even more encouraging and the existence of an inverse power law region is also apparent. No -5/3 power law (Kolmogorov, 1941) is evident in either Figure 1b or 1c; whereas, for the spectra measured in the fully-turbulent-region presented in Figure 22 of *PHC* a -5/3 power law region was clearly evident. Let us consider the lack of collapse at very low $k_1\Delta$ in Figure 1a in more detail.

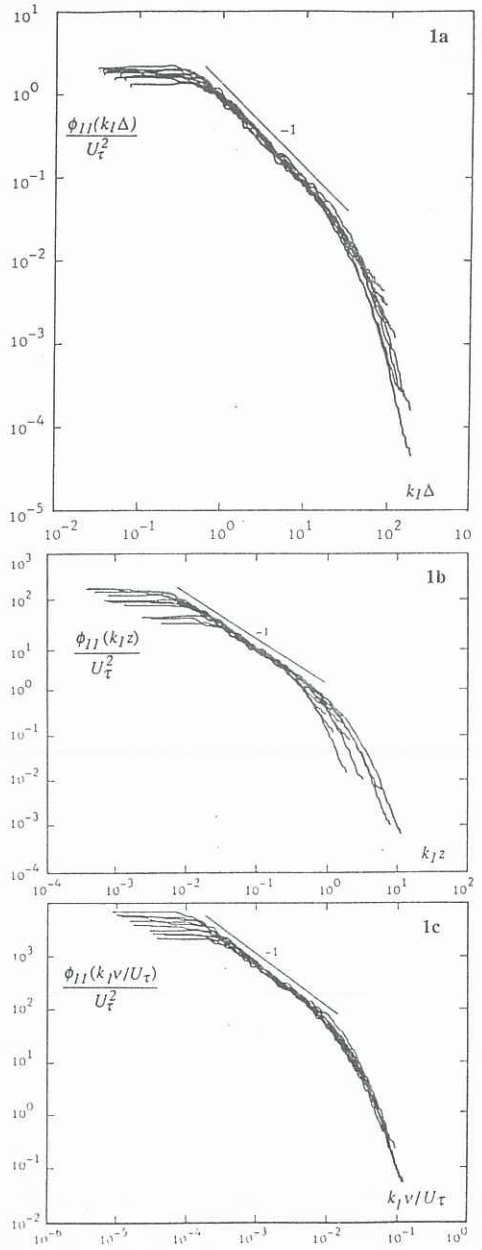

Figure 1 Near-wall pipe flow ϕ_{11}-spectra of Henbest (1983). (a) Outer-flow scaling, (b) Inner-flow scaling (c) Viscous scaling.

The value of $\phi_{11}(k_1\Delta)/U_\tau^2$ at low $k_1\Delta$ asymptotes to a constant value; let this be γ. It is expected that γ = constant for varying $z/\Delta \ll 1$ (see *PHC*). Figure 2 shows a plot of γ versus z^+ for different values of z/Δ for the near-wall data in Figure 1a and for the turbulent-wall-region data in Figure 22 of *PHC*. The value of γ appears to depend upon z^+ and not upon z/Δ, in the near-wall-region and this dependence extends into the turbulent-wall-region. This dependence of low wavenumber energy on viscous parameters should be treated cautiously and is not conclusive for the small range of z^+ and of z/Δ presented. There are a number of possible explanations for the observed behaviour in Figure 2.

(i) *PHC* attributed a similar lack of collapse in their turbulent-wall-region data to a convection velocity problem. In inferring k_1, a convection velocity, U_c, equal to the mean velocity at z was assumed. Let U_Δ denote the convection velocity of eddies of scale Δ and $(k_1)_{true}$ and $(\gamma)_{true}$ denote the true values of k_1 and γ, respectively. At low wavenumbers, $k_1 = (k_1)_{true}U_\Delta/U_c$ and therefore, $\gamma = (\gamma)_{true}U_c/U_\Delta$. An estimate of the ratio of γ at two values of z^+ owing to a spread in convection velocity is given by the ratio of the local mean velocities at the two values of z^+. This estimate is shown in Figure 2 by the dotted line and has been normalised to pass through γ for the lowest z^+ value for convenience. Clearly, a spread in convection velocity alone does not explain the variation in γ.

(ii) Spatial resolution of the hot-wire is not likely to enter the problem at such low wavenumbers. *PHC* measured ϕ_{11} with a 1.26mm wire and a 0.39mm wire (see their Figure 16b). The observed spread at low $k_1\Delta$ did not decrease with the shorter wire.

(iii) A possible explanation is that the action of viscosity attenuates the energy contribution of the large scale inactive motion, and as z^+ decreases the attenuation increases. This would suggest that the streamwise broad-band turbulence intensity in the near-wall-region is not universal with z^+ and depends in part on large scale inactive motions. Phillips (1990) came to a similar conclusion in his asymptotic analysis for the wall region of a turbulent boundary layer.

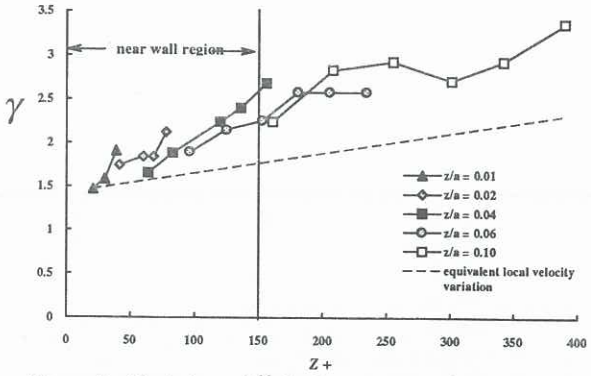

Figure 2 Variation of γ, the low wavenumber asymptote of $\phi_{11}(k_1\Delta)/U_\tau^2$, with z^+ for varying values of z/Δ for the data in Figure 1a and corresponding to the turbulent-wall-region data of *PHC*. Note here $\Delta = a$ = pipe radius.

5. BOUNDARY LAYER EXPERIMENT DETAILS

The wind tunnel and the smooth wall used in this experiment are described in Perry & Li (1990) and Li (1989). The pressure gradient variation along the working section length was less than 0.5%. Relevant boundary layer details are given in Table 1. Broadband turbulence intensities and the turbulence spectra were measured using constant-temperature hot-wire anemometers. Platinum Wollaston wire filaments (5 micron diameter, 1 mm length) were used

and operated at a resistance ratio of 2. The X-wires were nominally ± 45° to the free stream direction. Details of the matching and calibration procedure are similar to those given in Perry (1982) §8.6.1-8.6.4. The signal(s) was low pass filtered to prevent aliasing and sampled digitally and the spectrum was calculated using an FFT algorithm. The resulting spectrum spanned a frequency range of 0.2 Hz to 2kHz. The spectral argument was converted from frequency to one-dimensional streamwise wavenumber, k_1, using Taylor's (1938) hypothesis and each spectrum was normalised using (1). Some low Reynolds number boundary layer spectral data of Erm (1988) are presented in §6. Experimental details are given in Erm & Joubert (1991) and Table 1.

Boundary layer parameter	Present Experiment	Erm (1988)
$U\infty$ (m/s)	4.0	10.1
x from trip wire (mm)	3000	1940
Δ (mm)	80.41	36.67
U_τ (m/s), Clauser chart	0.169	0.412
ν/U_τ (mm)	0.0895	0.0371
$\Delta U_\tau/\nu$ = Kármán No	898	988
Trip wire diameter (mm)	3.00	1.20
Π (Coles, 1962)	0.44	0.517
R_θ	2081	2788

Table 1 Boundary layer details.

6. NEAR-WALL BOUNDARY LAYER SPECTRA

(i) ϕ_{11}, ϕ_{22}, and ϕ_{33} and ϕ_{13}-spectra

Figures 3a, b and c show the measured ϕ_{11}, ϕ_{22} and ϕ_{33} spectral data plotted with outer-flow scaling (2). Also plotted are the corresponding spectral data of Erm (1988). The inactive motion spectra, ϕ_{11} and ϕ_{22}, do not follow the expected collapse at low $k_1\Delta$ with viscous peel-offs at high $k_1\Delta$; instead, excellent collapse is seen at high $k_1\Delta$. The active motion spectra, ϕ_{33}, also collapse at high $k_1\Delta$. The reason for this collapse of ϕ_{11}, ϕ_{22} and ϕ_{33} at high $k_1\Delta$ is that the ratio of the boundary layer thickness to the viscous length scale, given by Kármán number = $\Delta U_\tau/\nu$, is fixed at 898 in the present results and 988 for Erm's results. This limited range of Kármán numbers is unfortunate. Furthermore, such low values of Kármán number for the boundary layer data prevent conclusions being made about outer-flow scaling at low wavenumber.

In Figure 4 the spectra in Figure 3 and Reynolds Shear stress spectra, $-\phi_{13}$, only for $\phi_{13} < 0$, are plotted with inner-flow scaling The ϕ_{11} spectra, Figure 4a, appear to collapse to a -5/3 power law region and no inverse power law region is evident, whereas, the ϕ_{22} spectra, Figure 4b, collapse to an inverse power law region and not to a -5/3 law region. The ϕ_{33} spectra, Figure 4c, do not collapse at low to moderate $k_1 z$ while a collapse of ϕ_{13} is more evident.

The spectral data in Figure 4 are shown with viscous scaling in Figure 5. Here, all spectra collapse well over a wide range of $k_1\nu/U_\tau$ from moderate to high $k_1\nu/U_\tau$. No inverse power law region is evident in ϕ_{11} or ϕ_{22}. The ϕ_{11}, ϕ_{33} and ϕ_{13} near-wall turbulent channel flow spectra of Antonia *et al.* (1991) also followed viscous scaling, (see their Figure 21a and 21b).

(ii) A note about Reynolds shear stress spectra

The measured ϕ_{13} changed sign from negative in the low to moderate wavenumber region to positive in the very high wavenumber region. This sign reversal has been noted by other workers. Champagne *et al.* (1970), from shear stress correlation measurements in nearly homogeneous turbulent shear flow, concluded that *'Lacking (for the moment, at least) a fluid-dynamic rationalization for this sign reversal, we might blame it on a systematic instrument error. Since correlation is a measure of phase angle, small differences between the phase shifts of the two channels could be the cause. A more likely cause is hot-wire spatial resolution difficulties ...'*. In the present data, u_1 and u_3 were measured simultaneously and hence no instrument-induced phase shift existed between u_1 and u_3. The near-wall co-spectrum measurements by Antonia *et al.* also gave a positive value of ϕ_{13} at very high wavenumbers (see their figure 21c). Also included in the same paper are direct numerical simulation results for turbulent channel flow. These results also showed a positive region of ϕ_{13} at very high wavenumbers (see their figure 22c). Thus it would seem that probe spatial resolution is not the cause. Antonia *et al.* suggested this positive value of ϕ_{13} corresponded to the negative production of turbulent energy in the high wavenumber region.

7. CONCLUSIONS AND DISCUSSION

Streamwise spectral data measured in the near-wall of pipe flow correlate well with the proposed spectral scaling laws. From an analysis of the data at low wavenumbers, it is tentatively proposed that the contributions from large scale inactive motions are attenuated in the near-wall-region by the action of viscosity . Near-wall boundary layer power spectra of the streamwise, spanwise and normal components of velocity and cross power spectra of Reynolds shear stress all collapse with viscous scaling at high wavenumber. The boundary layer spectra are quite different from the pipe flow spectra; and this difference is attributed to the low values of the Kármán number in the two boundary layer flows. In wall-bounded flows, mean flow quantities are normally used to determine whether the flow is fully developed; obviously, this is not an adequate criterion when considering turbulence quantities and spectra.

8. ACKNOWLEDGEMENTS

The authors would like to thank Dr. L.P. Erm of the Aeronautical Research Laboratory for providing the data from his Ph.D., and JDL & AEP thank the Australian Research Council for their financial support of this project.

9. REFERENCES

ANTONIA, R.A., TEITEL, M, KIM, J. & BROWNE, L.W.B. 1991 *J. Fluid Mech.*, **236**, 579-605.

CHAMPAGNE, F.H., HARRIS, V.G. & CORRSIN, S. 1970 *J. Fluid Mech.* **41**, 81-139.

COLES, D. 1962 . *U.S.A.F. The Rand Cooperation, Report R-403-PR*, Appendix A.

HENBEST, S.M. 1983 *The structure of turbulent pipe flow.* Ph.D. thesis, University of Melbourne, Australia.

ERM, L. P. 1988 *Low-Reynolds-number turbulent boundary layers.* Ph.D. thesis, University of Melbourne, Australia.

ERM, L. P. & JOUBERT, P. N. 1991 *J. Fluid Mech.*, **130**, 1-44.

KOLMOGOROV, A.N. 1941 *C.R. Acad. Sci. USSR*, **30**, 301.

LI, J. D. 1989 *The turbulence structure of wall shear flow.* Ph.D. thesis, University of Melbourne, Australia.

PERRY, A.E. 1982 *Hot-wire anemometry.* Clarendon Press Oxford.

PERRY, A.E. & ABELL, C.J. 1975 *J. Fluid Mech.*, **67**, 252-271.

PERRY, A.E. & ABELL, C.J. 1977 . *J. Fluid Mech.*, **79**, 785-799.

PERRY, A.E & CHONG, M.S. 1982 *J. Fluid Mech.*,. **119**, 173-217.

PERRY, A.E., HENBEST, S.M. & CHONG, M.S. 1986 *J. Fluid*

Mech., **165**, 163-199.
PERRY, A. E. & LI, J. D. 1990 *J. Fluid Mech.*, **218**, 405-438.
PHILLIPS, W.R.C. 1987 *Phys. Fluids*, **30**(B), 2354-2361.
ROBINSON, S.K. 1991 *Ann. Rev. Fluid Mech.*, **23**, 601-639.
SMITH, C.R., WALKER, J.D.A., HAIDARI, A.H. & SOBRUN, U. 1991 *Phil. Trans. Roy. Soc., London, Ser. A*, **336**, 131-175.
TAYLOR, G.I. 1938 *Proc. 5th Int. Congr. Appl. Mech.*, 291.
TOWNSEND, A.A. (1976) *The structure of turbulent shear flow*. 2nd ed., Cambridge University Press.

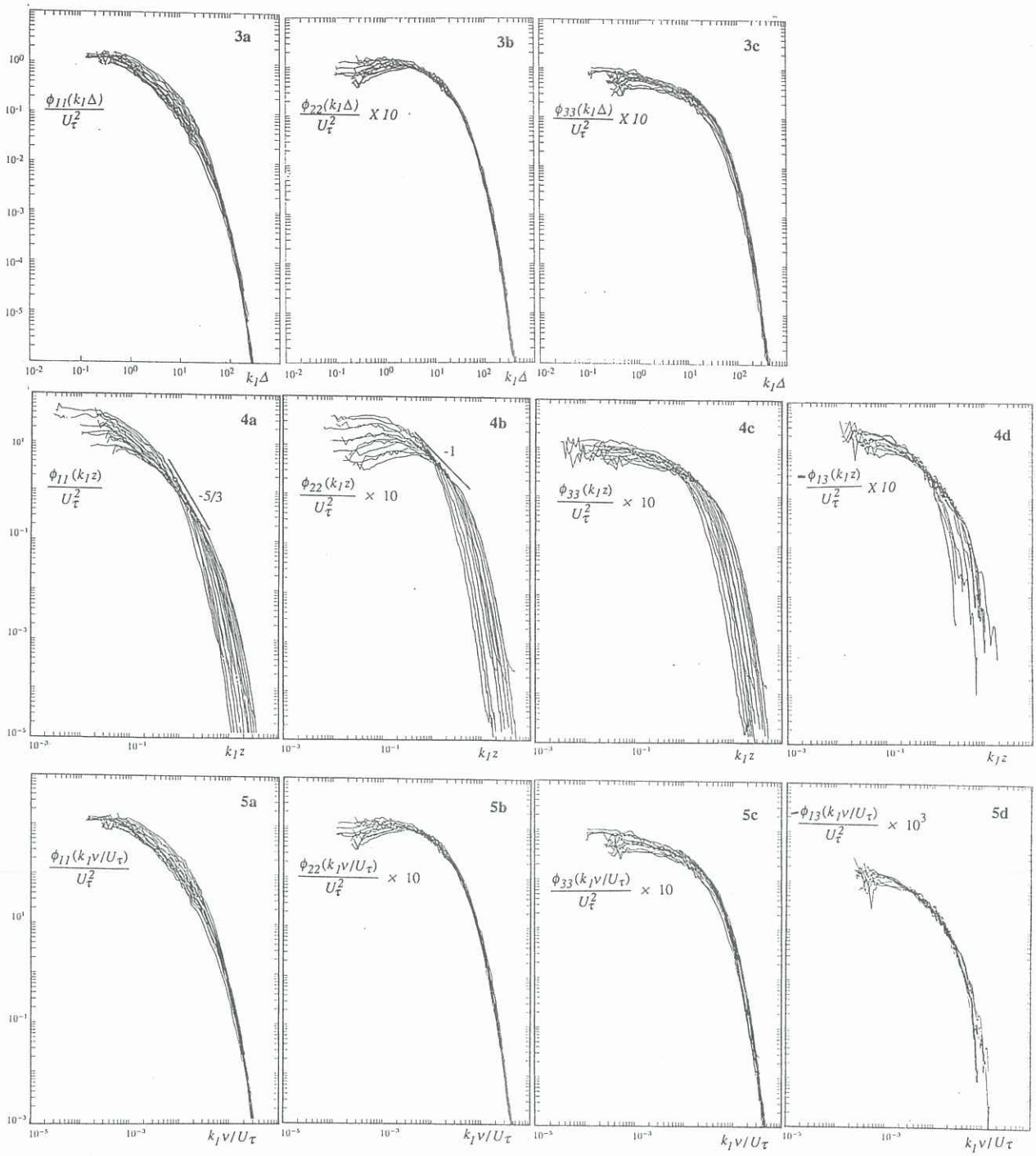

Figure 3 Spectra measured in the near wall region plotted with outer-flow scaling. Also shown are the spectra of Erm (1988). The range of z^+ was 30 to 150 and for $z/\Delta < 0.15$. (a) ϕ_{11}, (b) ϕ_{22}, (c) ϕ_{33}.

Figure 4 Spectra in Figure 3 plotted with inner-flow scaling. (a) ϕ_{11}, (b) ϕ_{22}, (c) ϕ_{33}. Reynolds shear stress spectra plotted with inner-flow scaling (d) $-\phi_{13}$ for $\phi_{13} < 0$.

Figure 5 Spectra in Figure 4 plotted with viscous scaling. (a) ϕ_{11}, (b) ϕ_{22}, (c) ϕ_{33}, (d) $-\phi_{13}$.